

$F_{\max} = 270$ GHz InAlN/GaN HEMT on Si with forming gas/nitrogen two-step annealing

Peng Cui¹, Meng Jia², Guangyang Lin¹, Jie Zhang¹, Lars Gundlach², and Yuping Zeng^{1*}

¹Department of Electrical and Computer Engineering, University of Delaware, Newark, DE 19716, USA

²Department of Chemistry and Biochemistry, University of Delaware, Newark, DE 19716, USA.

E-mail: yzeng@udel.edu

Abstract—In this letter, N₂ and forming gas (FG) were used during ohmic contact annealing of InAlN/GaN HEMTs on Si. It is found that N₂ annealing offers lower ohmic contact resistance (R_C) while FG annealing features lower sheet resistance (R_{sheet}). Then FG/N₂ two-step annealing was used to achieve a subthreshold swing (SS) of 113 mV/dec, an on/off current ($I_{\text{on}}/I_{\text{off}}$) ratio of $\sim 10^6$, a transconductance (g_m) peak of 415 mS/mm, a record low drain-inducing barrier lowering (DIBL) of 65 mV/V, and a record high power gain cutoff frequency (f_{\max}) of 270 GHz on 50-nm InAlN/GaN HEMT on Si.

Key words— InAlN/GaN HEMT, forming gas, ohmic contact annealing, cutoff frequency, Si substrate.

InAlN/GaN high-electron mobility transistor (HEMTs) on Si substrate have attracted extensive attentions ¹⁻⁶. Although Si substrate features a low cost and scaling capability than SiC substrate, the larger lattice mismatch between Si and GaN hindered the epitaxial material quality and device RF performance improvement. A high current gain cutoff frequency f_T of 400 GHz was achieved on a 30-nm InAlN/GaN HEMTs on SiC ⁷. A balanced current/power gain cutoff frequency f_T/f_{max} of 348/340 GHz (for E-mode device) and f_T/f_{max} of 302/301 GHz (for D-mode device) were demonstrated on 37-nm InAlN/GaN HEMTs on SiC ⁸. To date, f_T/f_{max} of 250/204 GHz ⁶ and f_T of 310 GHz ² were demonstrated on InAlN/GaN HEMTs on Si, respectively. This indicates that GaN-on-Si HEMTs technology needs to be drastically improved as compared to the GaN-on-SiC counterpart.

To improve device performance of InAlN/GaN HEMTs on Si, technology of fabrication process and material growth are the two keys. H₂/N₂ forming gas (FG) annealing has been widely used in the process manufacturing of GaN HEMTs ⁹⁻¹⁶. On one hand, FG can be used for the post-metallization annealing (PMA) to avoid unintentional oxidation, decrease leakage current, and reduce the traps by hydrogen passivation ⁹⁻¹². R. Wang *et al.* reported that a reverse gate leakage current of InAlN/GaN HEMT on SiC decreased from 10⁻⁷ to 10⁻¹² A/mm after PMA and a record high on/off current (I_{on}/I_{off}) ratio of 10¹² was achieved ¹⁰. On the other hand, FG annealing can also be used to form ohmic contact ¹³⁻¹⁶.

In this letter, N₂ and forming gas (FG) were used in ohmic contact annealing in InAlN/GaN HEMTs on Si. It is found that N₂ annealing offers lower ohmic contact

resistance (R_C) while FG annealing features lower sheet resistance (R_{sheet}). X-ray photoelectron spectra (XPS) showed that FG annealing can remove the surface native oxide, leading to a reduced material sheet resistance. Then a process using FG/N₂ two-step annealing was developed, and a reduced subthreshold swing (SS), an improved transconductance (g_m), a record low drain-inducing barrier lowering (DIBL) of 65 mV/V, as well as a f_T/f_{max} of 125/270 GHz was achieved on 50-nm InAlN/GaN HEMT, resulting in a high $(f_T \times f_{\text{max}})^{1/2}$ of 184 GHz among GaN HEMTs on Si.

The epitaxial layer used in this letter was grown by metal organic chemical vapor deposition (MOCVD) on 4-inch Si substrate. It consists of 2-nm GaN cap layer, an 8-nm lattice-matched In_{0.17}Al_{0.83}N barrier layer, a 1-nm AlN interlayer, a 15-nm GaN channel layer, a 4-nm In_{0.12}Ga_{0.88}N back barrier layer, and a 2- μm undoped GaN buffer layer. Device fabrication started with mesa isolation using Cl₂-based inductively coupled plasma etching. Ti/Al/Ni/Au stack was deposited and annealed to form alloyed ohmic contacts. The ohmic contact rapid thermal annealing (RTA) process was carried out using Solaris 150 Rapid Thermal Processing System with a ramping speed of 50°C/s. The system temperature accuracy and stability is $\pm 2.5^\circ\text{C}$ and the temperature variation across the entire chamber is $\pm 2.5^\circ\text{C}$. Three different types of ohmic contact annealing processes were used on three samples. Sample 1 is annealed at 850°C for 40s in N₂. Sample 2 is annealed at 850°C for 40s in forming gas (FG: 5% H₂ and 95% N₂). Sample 3 is annealed at 850°C first in FG for 20s and then in N₂ for 20s. Then these three samples were treated using oxygen plasma treatment. Finally, a Ni/Au T-shaped gate with a gate width (W_g) of $2 \times 20 \mu\text{m}$ was fabricated by electron beam lithography. The

devices present a source-drain spacing (L_{sd}) of 1 μm , a gate-source spacing (L_{gs}) of 475 nm, and a gate footprint (L_g) of 50 nm, respectively. No passivation process was applied on the reported devices.

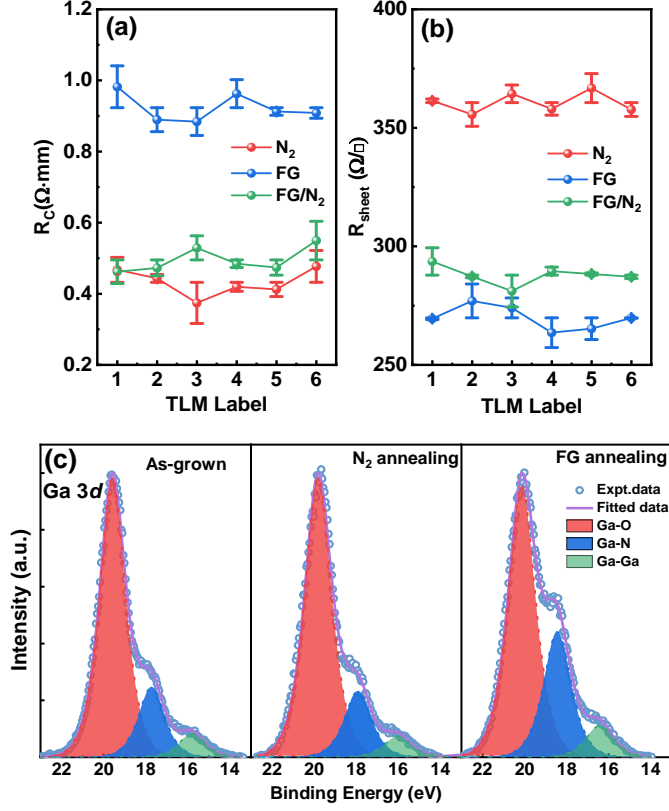


Table I	R_C	R_{sheet}	n_{2D}	μ
	($\Omega \cdot \text{mm}$)	(Ω/\square)	(cm^{-2})	($\text{cm}^2/\text{V} \cdot \text{s}$)
Sample 1 (N_2)	0.43	361	1.87×10^{13}	928
Sample 2 (FG)	0.92	270	2.15×10^{13}	1077
Sample 3 (FG/ N_2)	0.49	288	2.11×10^{13}	1028

Fig. 1. (a) Ohmic contact resistance (R_C) and (b) sheet resistance (R_{sheet}) under N_2 annealing, forming gas (FG) annealing, and FG/ N_2 two-step annealing with six sets of TLM patterns (“I” represents the error bar). (c) XPS spectra of Ga 3d core-level taken from as-grown sample and samples after annealing in N_2 , and FG, respectively. Table I: the average values of R_C and R_{sheet} , electron density (n_{2D}), and electron mobility (μ) under different annealing conditions.

The DC current-voltage (I - V) measurements were carried out by using an Agilent B1500A semiconductor parameter analyzer. Fig. 1(a) and (b) shows the Ohmic contact resistance (R_C) and sheet resistance (R_{sheet}) for three types annealing conditions obtained using six sets of TLM patterns. The average values of R_C and R_{sheet} (shown in Table I) are $0.43 \text{ } \Omega \cdot \text{mm}/361 \text{ } \Omega/\square$ (N_2 annealing), $0.92 \text{ } \Omega \cdot \text{mm}/269 \text{ } \Omega/\square$ (FG annealing), and $0.49 \text{ } \Omega \cdot \text{mm}/288 \text{ } \Omega/\square$ (FG/ N_2 annealing), respectively. N_2 annealing showed the lowest R_C and highest R_{sheet} , and FG annealing presented the opposite behavior. Fig. 1(c) compares the X-ray photoelectron spectra (XPS) of Ga $3d$ core-level taken from as-grown sample (without annealing) and samples after annealing in N_2 and FG. The spectra can be resolved into three peaks. The fitting peaks at around 20, 18, and 16 eV binding energies are attributed to Ga-O, Ga-N, and Ga-Ga bonds, respectively¹⁷⁻¹⁹. The chemical component change of the sample after N_2 annealing can be neglected compared to that of the as-grown sample; while for the sample with FG annealing, the Ga-O component significantly decreases and Ga-N component increases, compared to those in the as-grown sample. The results indicate that FG annealing can effectively remove the low quality native oxide (GaO_x) and form a nitridation interlayer¹⁹⁻²¹. As shown in Table I, two-dimensional electron gas (2DEG) electron density (n_{2D}) extracted from capacitance-voltage measurement increased from $1.87 \times 10^{13} \text{ cm}^{-2}$ (N_2) to $2.15 \times 10^{13} \text{ cm}^{-2}$ (FG), presenting a 15% increase. Based on the R_{sheet} and n_{2D} , the 2DEG electron mobility (μ) can be calculated and showed a 16% increase with FG annealing, an indication of an improved material surface quality with a weakened remote surface charge scattering²²⁻²⁵. However, the increased R_C from FG annealing degrades the

device performance. In order to benefit from the good material property due to FG annealing and the low R_C due to N_2 annealing, FG/ N_2 two-step annealing was applied on Sample 3 and a compromised characteristic was obtained.

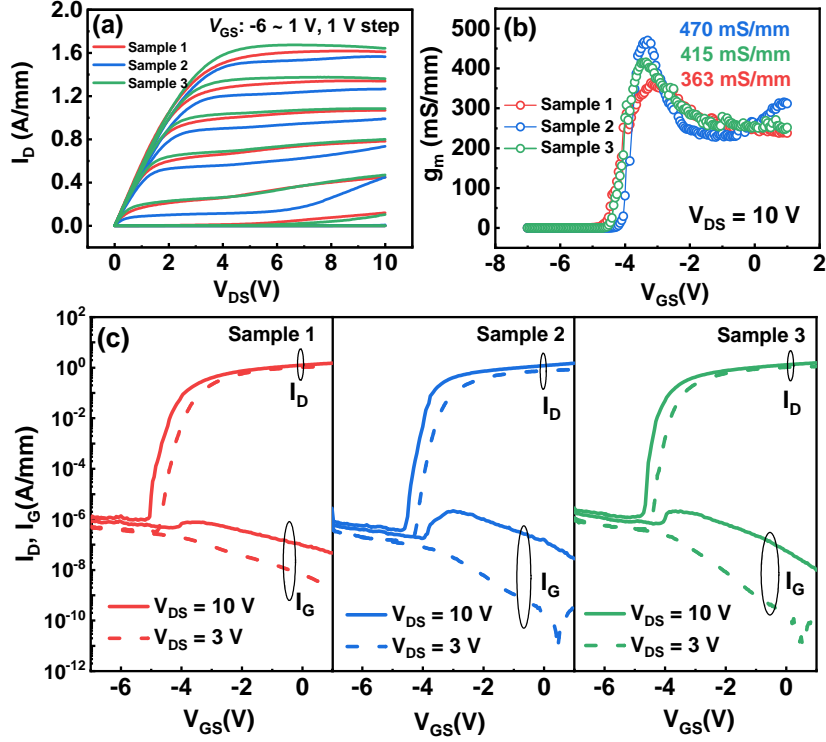


Fig. 2. (a) I - V output characteristic; (b) extrinsic transconductance, (c) transfer curves and gate current curves in semi-log scale at $V_{DS} = 10$ and 3 V of the three samples.

Fig. 2(a) shows the I - V output characteristics of the 50-nm InAlN/GaN HEMTs. The device on-resistances (R_{on}) extracted at gate-source voltage (V_{GS}) of 0 V and drain-source voltage (V_{DS}) in the range between 0 and 0.5 V are $1.77 \Omega \cdot \text{mm}$ (Sample 1), $2.02 \Omega \cdot \text{mm}$ (Sample 2), and $1.82 \Omega \cdot \text{mm}$ (Sample 3), respectively. The discrepancy of R_{on} values with those calculated from TLM results should come from the Asher oxidation treatment prior to gate metal deposition, which can oxidize the material surface and then change the channel resistance. The maximum saturation drain currents (I_D) at $V_{GS} = 1$ V and $V_{DS} = 10$ V are 1.61, 1.57 and 1.64 A/mm for the three samples. The lowest

saturation I_D of Sample 2 is due to the high R_C . The removed native oxide can effectively increase n_s and gate capacitance, therefore, Sample 3 features the highest saturation I_D . Fig. 2(b) shows the extracted extrinsic transconductance (g_m) at $V_{DS} = 10$ V. Compared to g_m peak of Sample 1 (363 mS/mm), Samples 2 and 3 showed higher g_m peak of 470 and 415 mS/mm, respectively, leading to the improved g_m achieved with FG annealing. FG annealing removed the low quality native oxide and reduced gate-to-channel distance, leading to the increased g_m peak. However, the FG/N₂ two-step annealing can increase the nitridation layer, which can increase gate-to-channel distance. Therefore, a slightly decreased g_m compared with that of Sample 2 was observed. Fig. 2(c) shows the transfer characteristics and gate current (I_G) curves of three samples in semi-log scale at V_{DS} of 10 V and 3 V, respectively. At $V_{DS} = 10$ V, on/off current (I_{on}/I_{off}) ratio of three samples were $\sim 10^6$ and an improved subthreshold swing (SS) were observed (Samples 1-3: 237, 166, 113 mV/dec, respectively). The drain-inducing barrier lowering (DIBL) of 69, 65, and 65 mV/V were extracted at $I_D = 10$ mA/mm between $V_{DS} = 10$ V and $V_{DS} = 3$ V. To the best of our knowledge, this is the lowest value (65 mV/V) among all GaN HEMTs on Si. The breakdown voltage (BV_{DS}) of 20 V for three sample was determined at $I_D = 1$ mA/mm when V_{GS} was fixed at -8 V.

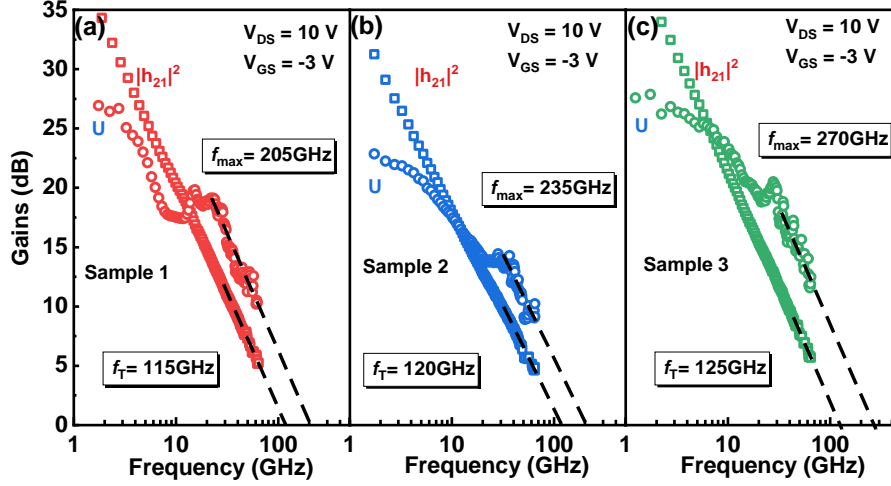


Fig. 3. RF performance of 50-nm InAlN/GaN HEMT at $V_{GS} = -3$ V and $V_{DS} = 10$ V with (a) f_T/f_{max} of 115/205 GHz for Sample 1, (b) f_T/f_{max} of 120/210 GHz for Sample 2, and (c) f_T/f_{max} of 125/270 GHz for Sample 3.

The RF measurement was taken with Anritsu MS4647B vector network analyzer configured to operate from 1 to 65 GHz. The network analyzer was calibrated using Line Reflect Match (LRM) calibration. On-wafer open and short structures were used to eliminate the effects of parasitic elements. After de-embedding, the current gain $|h_{21}|^2$ and unilateral gain U as a function of frequency at $V_{DS} = 10$ V, $V_{GS} = -3$ V were shown in Fig. 3. f_T/f_{max} of 115/205, 120/210, 125/270 GHz for three samples are extracted using extrapolation of $|h_{21}|^2$ with a -20 dB/dec slope, resulting in $f_T \cdot L_g$ of 5.75, 6, and 6.25 GHz $\cdot \mu\text{m}$, respectively. Here $(f_T \times f_{max})^{1/2}$ of 154, 159, and 184 GHz were obtained for the three samples. With FG/N₂ two-step annealing, f_T increased slightly but f_{max} presented a drastic improvement. Compared with FG annealing, the FG/N₂ two-step annealing can facilitate the formation of nitridation interlayer. The nitrogen atoms can effectively decrease the O vacancies from the removal of native oxide and offered better material interface¹⁹⁾, which improves the device performance. To the best of our

knowledge, this is the highest f_{\max} among reported GaN HEMTs on Si, as shown in Fig.

4.

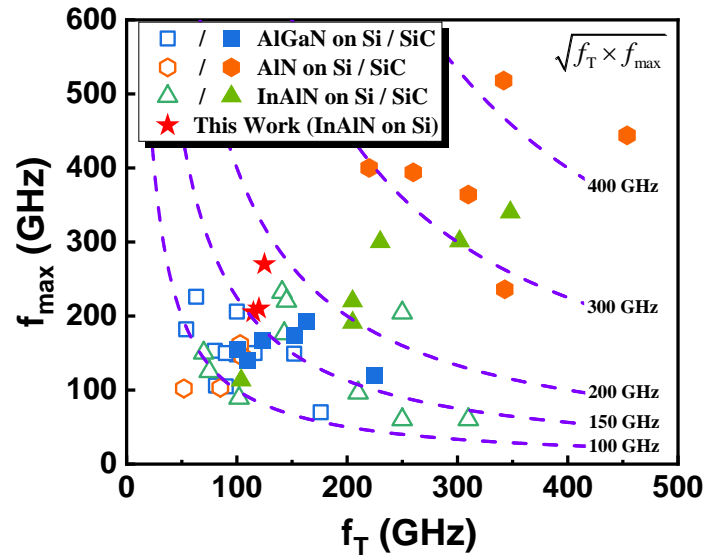


Fig. 4. Comparison of f_T/f_{\max} of the InAlN/GaN HEMTs on Si in this work with other reported GaN HEMTs (AlGaN on Si²⁶⁻³⁶/SiC³⁷⁻⁴⁰), AlN on Si⁴¹⁻⁴³/SiC⁴⁴⁻⁴⁸), and InAlN on Si^{2, 4, 49-54}/SiC⁵⁵⁻⁵⁹).

In summary, the 50-nm InAlN/GaN HEMT with FG/N₂ annealing exhibits an $I_{\text{on}}/I_{\text{off}}$ ratio of 10^6 , a g_m peak of 415 mS/mm, an average SS of 113 mV/dec, and a DIBL of 65 mV/V. RF measurement of the 50-nm InAlN/GaN HEMT presents a f_T/f_{\max} of 125/270 GHz and an $(f_T \times f_{\max})^{1/2}$ of 184 GHz. The fabrication technology for GaN HEMTs on Si yields excellent RF characteristics, which shows the great application potential of GaN-on-Si for millimeter wave power amplifiers.

Reference

- 1) D. Marti, S. Tirelli, V. Teppati, L. Lugani, J.-F. Carlin, M. Malinverni, N. Grandjean and C.R. Bolognesi, *IEEE Electron Device Lett.* **36** (1), 17 (2014).
- 2) H. Xie, Z. Liu, Y. Gao, K. Ranjan, K.E. Lee and G.I. Ng, *Appl. Phys. Express* **12** (12), 126506 (2019).
- 3) W. Xing, Z. Liu, H. Qiu, K. Ranjan, Y. Gao, G.I. Ng and T. Palacios, *IEEE Electron Device Lett.* **39** (1), 75 (2017).
- 4) H. Xie, Z. Liu, Y. Gao, K. RANJAN, K.E. Lee and G.I. Ng, *Appl. Phys. Express* (2019).
- 5) P. Cui, A. Mercante, G. Lin, J. Zhang, P. Yao, D.W. Prather and Y. Zeng, *Appl. Phys. Express* **12** (10), 104001 (2019).
- 6) L. Li, K. Nomoto, M. Pan, W. Li, A. Hickman, J. Miller, K. Lee, Z. Hu, S.J. Bader and S.M. Lee, *IEEE Electron Device Lett.* **41** (5), 689 (2020).
- 7) Y. Yue, Z. Hu, J. Guo, B. Sensale-Rodriguez, G. Li, R. Wang, F. Faria, B. Song, X. Gao and S. Guo, *Jpn. J. Appl. Phys.* **52** (8S), 08JN14 (2013).
- 8) M.L. Schuette, A. Ketterson, B. Song, E. Beam, T.-M. Chou, M. Pilla, H.-Q. Tserng, X. Gao, S. Guo and P.J. Fay, *IEEE Electron Device Lett.* **34** (6), 741 (2013).
- 9) Y.-S. Lin, Y.-W. Lain and S.S. Hsu, *IEEE Electron Device Lett.* **31** (2), 102 (2009).
- 10) R. Wang, P. Saunier, Y. Tang, T. Fang, X. Gao, S. Guo, G. Snider, P. Fay, D. Jena and H. Xing, *IEEE Electron Device Lett.* **32** (3), 309 (2011).
- 11) T. Kawanago, K. Kakushima, Y. Kataoka, A. Nishiyama, N. Sugii, H. Wakabayashi, K. Tsutsui, K. Natori and H. Iwai, *IEEE Trans. Electron Devices* **61** (3), 785 (2014).
- 12) S. Kumar, P. Gupta, I. Guiney, C.J. Humphreys, S. Raghavan, R. Muralidharan and D.N. Nath, *IEEE Trans. Electron Devices* **64** (12), 4868 (2017).
- 13) H. Sun, A.R. Alt, H. Benedickter, C. Bolognesi, E. Feltrin, J.-F. Carlin, M. Gonschorek, N. Grandjean, T. Maier and R. Quay, *IEEE Electron Device Lett.* **30** (8), 796 (2009).
- 14) A. Chini, D. Buttari, R. Coffie, L. Shen, S. Heikman, A. Chakraborty, S. Keller and U. Mishra, *IEEE Electron Device Lett.* **25** (5), 229 (2004).
- 15) D. Marti, C. Bolognesi, Y. Cordier, M. Chmielowska and M. Ramdani, *Appl. Phys. Express* **4** (6), 064105 (2011).
- 16) D. Buttari, A. Chini, G. Meneghesso, E. Zanoni, P. Chavarkar, R. Coffie, N. Zhang, S. Heikman, L.

- Shen, H. Xing, C. Zheng and a.U.K. Mishra, *IEEE Electron Device Lett.* **23** (3), 118 (2002).
- 17) M. Mishra, S.K. TC, N. Aggarwal, M. Kaur, S. Singh and G. Gupta, *Phys. Chem. Chem. Phys.* **17** (23), 15201 (2015).
- 18) Q. Wang, X. Cheng, L. Zheng, L. Shen, J. Li, D. Zhang, R. Qian and Y. Yu, *RSC advances* **7** (19), 11745 (2017).
- 19) S. Yang, Z. Tang, K.-Y. Wong, Y.-S. Lin, C. Liu, Y. Lu, S. Huang and K.J. Chen, *IEEE Electron Device Lett.* **34** (12), 1497 (2013).
- 20) C. Hinkle, M. Milojevic, B. Brennan, A.M. Sonnet, F. Aguirre-Tostado, G. Hughes, E. Vogel and R. Wallace, *Appl. Phys. Lett.* **94** (16), 162101 (2009).
- 21) S. Huang, Q. Jiang, S. Yang, C. Zhou and K.J. Chen, *IEEE Electron Device Lett.* **33** (4), 516 (2012).
- 22) M. Marso, G. Heidelberger, K.M. Indlekofer, J. Bernát, A. Fox, P. Kordos and H. Luth, *IEEE Trans. Electron Devices* **53** (7), 1517 (2006).
- 23) T.-H. Hung, P.S. Park, S. Krishnamoorthy, D.N. Nath and S. Rajan, *IEEE Electron Device Lett.* **35** (3), 312 (2014).
- 24) T.-H. Hung, M. Esposito and S. Rajan, *Appl. Phys. Lett.* **99** (16), 162104 (2011).
- 25) D. Ji, B. Liu, Y. Lu, G. Liu, Q. Zhu and Z. Wang, *Appl. Phys. Lett.* **100** (13), 132105 (2012).
- 26) S. Tirelli, D. Marti, H.F. Sun, A.R. Alt, H. Benedickter, E.L. Piner and C.R. Bolognesi, *IEEE Electron Device Lett.* **31** (4), 296 (2010).
- 27) D. Marti, S. Tirelli, A.R. Alt, J. Roberts and C. Bolognesi, *IEEE Electron Device Lett.* **33** (10), 1372 (2012).
- 28) S. Bouzid-Driad, H. Maher, N. Defrance, V. Hoel, J.-C. De Jaeger, M. Renvoise and P. Frijlink, *IEEE Electron Device Lett.* **34** (1), 36 (2012).
- 29) A. Soltani, J.C. Gerbedoen, Y. Cordier, D. Ducatteau, M. Rousseau, M. Chmielowska, M. Ramdani and J.C. De Jaeger, *IEEE Electron Device Lett.* **34** (4), 490 (2013).
- 30) S. Huang, K. Wei, G. Liu, Y. Zheng, X. Wang, L. Pang, X. Kong, X. Liu, Z. Tang and S. Yang, *IEEE Electron Device Lett.* **35** (3), 315 (2014).
- 31) Y. Murase, K. Asano, I. Takenaka, Y. Ando, H. Takahashi and C. Sasaoka, *IEEE Electron Device Lett.* **35** (5), 524 (2014).
- 32) W. Jatal, U. Baumann, K. Tonisch, F. Schwierz and J. Pezoldt, *IEEE Electron Device Lett.* **36** (2), 123 (2015).

- 33) P. Altuntas, F. Lecourt, A. Cutivet, N. Defrance, E. Okada, M. Leseq, S. Rennesson, A. Agboton, Y. Cordier, V. Hoel and J.C. De Jaeger, *IEEE Electron Device Lett.* **36** (4), 303 (2015).
- 34) S. Bouzid, H. Maher, N. Defrance, V. Hoel, F. Lecourt, M. Renvoise, J.C. De Jaeger and P. Frijlink, *Electron. Lett.* **48** (2), 69 (2012).
- 35) P. Christy, Y. Katayama, A. Wakejima and T. Egawa, *Electron. Lett.* **51** (17), 1366 (2015).
- 36) H. Sun, A. Alt, H. Benedickter and C. Bolognesi, *Electron. Lett.* **45** (7), 376 (2009).
- 37) M. Micovic, N. Nguyen, P. Janke, W.-S. Wong, P. Hashimoto, L.-M. McCray and C. Nguyen, *Electron. Lett.* **36** (4), 358 (2000).
- 38) W. Lu, J. Yang, M.A. Khan and I. Adesida, *IEEE Trans. Electron Devices* **48** (3), 581 (2001).
- 39) M. Higashiwaki, T. Matsui and T. Mimura, *IEEE Electron Device Lett.* **27** (1), 16 (2005).
- 40) J.W. Chung, T.-W. Kim and T. Palacios: 2010 International Electron Devices Meeting, 2010, p. 30.2. 1.
- 41) F. Medjdoub, N. Waldhoff, M. Zegaoui, B. Grimbert, N. Rolland and P. Rolland, *IEEE Electron Device Lett.* **32** (9), 1230 (2011).
- 42) F. Medjdoub, Y. Tagro, M. Zegaoui, B. Grimbert, F. Danneville, D. Ducatteau, N. Rolland and P.A. Rolland, *IEEE Electron Device Lett.* **33** (9), 1258 (2012).
- 43) F. Medjdoub, M. Zegaoui and N. Rolland, *Electron. Lett.* **47** (24), 1345 (2011).
- 44) K. Shinohara, D.C. Regan, Y. Tang, A.L. Corrion, D.F. Brown, J.C. Wong, J.F. Robinson, H.H. Fung, A. Schmitz and T.C. Oh, *IEEE Trans. Electron Devices* **60** (10), 2982 (2013).
- 45) K. Shinohara, D. Regan, A. Corrion, D. Brown, S. Burnham, P. Willadsen, I. Alvarado-Rodriguez, M. Cunningham, C. Butler and A. Schmitz: 2011 International Electron Devices Meeting, 2011, p. 19.1. 1.
- 46) K. Shinohara, A. Corrion, D. Regan, I. Milosavljevic, D. Brown, S. Burnham, P. Willadsen, C. Butler, A. Schmitz and D. Wheeler: 2010 International Electron Devices Meeting, 2010, p. 30.1. 1.
- 47) K. Shinohara, D. Regan, I. Milosavljevic, A. Corrion, D. Brown, P. Willadsen, C. Butler, A. Schmitz, S. Kim and V. Lee, *IEEE Electron Device Lett.* **32** (8), 1074 (2011).
- 48) K. Shinohara, D. Regan, A. Corrion, D. Brown, Y. Tang, J. Wong, G. Candia, A. Schmitz, H. Fung and S. Kim: 2012 International Electron Devices Meeting, 2012, p. 27.2. 1.
- 49) H.F. Sun, A.R. Alt, H. Benedickter, C.R. Bolognesi, E. Feltin, J.F. Carlin, M. Gonschorek, N. Grandjean, T. Maier and R. Quay, *IEEE Electron Device Lett.* **30** (8), 796 (2009).

- 50) D. Marti, S. Tirelli, V. Teppati, L. Lugani, J.F. Carlin, M. Malinverni, N. Grandjean and C.R. Bolognesi, *IEEE Electron Device Lett.* **36** (1), 17 (2015).
- 51) W. Xing, Z. Liu, H. Qiu, K. Ranjan, Y. Gao, G.I. Ng and T. Palacios, *IEEE Electron Device Lett.* **39** (1), 75 (2018).
- 52) C.-W. Tsou, C.-Y. Lin, Y.-W. Lian and S.S. Hsu, *IEEE Trans. Electron Devices* **62** (8), 2675 (2015).
- 53) H. Ichikawa, C. Mizue, I. Makabe, Y. Tateno, K. Nakata and K. Inoue: 2014 Asia-Pacific Microwave Conference, 2014, p. 780.
- 54) S. Arulkumaran, G.I. Ng, K. Ranjan, C.M.M. Kumar, S.C. Foo, K.S. Ang, S. Vicknesh, S.B. Dolmanan, T. Bhat and S. Tripathy, *Jpn. J. Appl. Phys.* **54** (4S), 04DF12 (2015).
- 55) K.D. Chabak, M. Trejo, A. Crespo, D.E. Walker, J. Yang, R. Gaska, M. Kossler, J.K. Gillespie, G.H. Jessen and V. Trimble, *IEEE Electron Device Lett.* **31** (6), 561 (2010).
- 56) M.L. Schuette, A. Ketterson, B. Song, E. Beam, T.-M. Chou, M. Pilla, H.-Q. Tserng, X. Gao, S. Guo and P.J. Fay, *IEEE Electron Device Lett.* **34** (6), 741 (2013).
- 57) H. Sun, A.R. Alt, H. Benedickter, E. Feltin, J.-F. Carlin, M. Gonschorek, N.R. Grandjean and C. Bolognesi, *IEEE Electron Device Lett.* **31** (9), 957 (2010).
- 58) S. Tirelli, D. Marti, H. Sun, A.R. Alt, J.-F. Carlin, N. Grandjean and C. Bolognesi, *IEEE Electron Device Lett.* **32** (10), 1364 (2011).
- 59) R. Wang, G. Li, G. Karbasian, J. Guo, B. Song, Y. Yue, Z. Hu, O. Laboutin, Y. Cao and W. Johnson, *IEEE Electron Device Lett.* **34** (3), 378 (2013).